Available online at www.sciencedirect.com
ScienceDirect
Journal of Power Sources 177 (2008) 104–110
JOURNAL OF POWER SOURCES
www.elsevier.com/locate/jpowsour

Implications of electronic short circuiting in plasma sprayed solid oxide fuel cells on electrode performance evaluation by electrochemical impedance spectroscopy

B.D. White [a], O. Kesler [b,*]

[a] *Department of Mechanical Engineering, The University of British Columbia, 2054-6250 Applied Sciences Lane, Vancouver, British Columbia, Canada V6T 1Z4*
[b] *Department of Mechanical and Industrial Engineering, University of Toronto, 5 King's College Road, Toronto, Ontario, Canada M5S 3G8*

Received 8 September 2007; received in revised form 4 November 2007; accepted 5 November 2007
Available online 17 November 2007

Abstract

Electronic short circuiting of the electrolyte in a solid oxide fuel cell (SOFC) arising from flaws in the plasma spray fabrication process has been found to have a significant effect on the perceived performance of the electrodes, as evaluated by electrochemical impedance spectroscopy (EIS). The presence of a short circuit has been found to lead to the underestimation of the electrode polarization resistance (R_p) and hence an overestimation of electrode performance. The effect is particularly noticeable when electrolyte resistance is relatively high, for example during low to intermediate temperature operation, leading to an obvious deviation from the expected Arrhenius-type temperature dependence of R_p. A method is developed for determining the real electrode performance from measurements of various cell properties, and strategies for eliminating the occurrence of short circuiting in plasma sprayed cells are identified.

Keywords: Solid oxide fuel cells; Plasma spraying; Composite cathode; LSM; Impedance spectroscopy

1. Introduction

Plasma spraying of both individual solid oxide fuel cell (SOFC) components and entire cells has been applied by many investigators to overcome some of the limitations of conventional manufacturing processes [1]. In plasma spray processing, an electric arc is used to heat and ionize a mixture of gasses, typically including argon, nitrogen, and hydrogen or helium, to produce an energetic plasma. These gasses are fed into the torch in varying proportions, depending on the desired properties of the plasma. Particles of the material to be sprayed are then fed into the hot plasma where they absorb heat and are accelerated towards the substrate at speeds of up to 500 m s^{-1}. The most obvious advantage of plasma spraying is the speed of fabrication that can be realized by significantly reducing, or eliminating completely, the need for sintering of the cell components. This allows the cell layers to be quickly deposited in succession. The plasma spray process is also easily automated and has been applied successfully in industrial scale mass production settings in the manufacturing of ceramic coatings for a wide variety of applications [2,3]. Furthermore, the elimination of high-temperature sintering greatly simplifies the use of metal interconnects as cell supports, further reducing material costs. It also reduces the opportunity for undesired inter-reactions between cell components, thus enhancing durability.

In spite of the many potential advantages, the use of plasma spraying introduces significant challenges in the manufacture of the highest quality SOFCs. These challenges largely relate to the types of coating microstructures that result from the plasma spray process and their suitability for use as SOFC components. This situation is further complicated by the significantly different requirements for these various components. SOFC electrodes require high levels of open porosity (~40%)

* Corresponding author. Tel.: +1 416 978 3835; fax: +1 416 978 7753.
E-mail addresses: bdwhite@interchange.ubc.ca (B.D. White), kesler@mie.utoronto.ca (O. Kesler).

0378-7753/$ – see front matter © 2007 Elsevier B.V. All rights reserved.
doi:10.1016/j.jpowsour.2007.11.014

to allow for the transport of reaction gasses and high internal surface area to provide a large number of reaction sites. In the case of composite SOFC electrodes, these properties must be achieved with the simultaneous deposition of two or more materials having very different melting temperatures, for example lanthanum strontium manganite (LSM) and yttria-stabilized zirconia (YSZ). SOFC electrolytes, on the other hand, must have very low levels of porosity (<1%) to prevent gas leakage, while being as thin as possible.

The properties of the substrate and deposited coatings can also have an influence on the quality of coatings deposited afterwards. For example, conditions generally favourable for the deposition of high performance electrodes can result in the presence of a few relatively large, un-melted ceramic particles in these coatings together with large pores [4]. Perhaps more significantly, the need for gas permeability through the substrate requires that the substrate surface be relatively porous and therefore uneven. This type of open surface porosity poses challenges for deposition of the succeeding electrode and electrolyte layers, and can lead to the presence of significant flaws in the coatings. One such resulting flaw that has been observed in this work in some SOFCs fabricated by air plasma spraying (APS) is the presence of an electronic short circuit between the cell's electrodes, through the electrolyte. This flaw not only reduces the performance and efficiency of the SOFC by reducing the cell voltage, but it can also have the less intuitive effect of lowering the apparent polarization resistance (R_p^{app}) of the SOFC electrodes as measured by electrochemical impedance spectroscopy (EIS). This second effect could lead to misjudging the performance of electrodes to be higher than is actually the case, particularly when evaluating electrodes in symmetric cell configurations where measurements of full cell voltage are not possible.

The result of this manufacturing flaw is analogous to the presence of electronic conductivity in mixed ionic and electronic conducting (MIEC) electrolyte materials, which has been previously reported to have the effect of decreasing the apparent R_p in EIS measurements [5,6]. The presence of a manufacturing flaw leading to physical short circuiting in plasma sprayed coatings, however, has the potential to have a much more significant effect on apparent R_p than would normally be the case in MIEC electrolytes due to the high electronic conductivity of the short circuit path compared to the ionic conductivity of the electrolyte. This combination has the potential to result in significant overestimation of electrode performance, particularly at low temperatures, and can even, in the most extreme cases, cause the apparent R_p of electrodes to *increase* with increasing temperature. For this reason, the detection and identification of any effects caused by manufacturing-induced short circuit flaws is critically important in the development and characterization of electrode processing techniques.

This article discusses the fabrication by APS and analysis, both electrochemical and microstructural, of cathode symmetric cells that exhibit electronic short circuiting across the electrolyte. We also derive an expression that quantifies the magnitude of the effect of this short circuit on the apparent R_p of the electrodes and allows the real electrode performance to be determined from electrochemical test data and physical cell parameters. Finally, improved cell manufacturing processes are discussed that correct the manufacturing flaw and eliminate electronic short circuiting within the cell.

2. Experimental method

2.1. Plasma spray processing

The deposition of the SOFC cathode symmetric cells used in this work was carried out using an Axial III Series 600 axial injection APS torch with three cathodes (Northwest Mettech Corp., North Vancouver, BC, Canada). LSM/YSZ composite cathodes were deposited, along with 10 mol% YSZ electrolytes, onto commercially available porous 1 in. diameter 430 stainless steel (SS) substrates, fabricated by powder metallurgy (Media Grade 5, Mott Corporation, Farmington, Connecticut). These substrates were selected as they were found to have a sufficiently rough surface that allowed for adequate adhesion of coatings deposited over a wide range of conditions, and were sufficiently porous to allow for gas transport to the electrodes. These substrates were mounted on a rotating turntable spinning at 400 rpm to prevent overheating during the deposition process.

In each symmetric cell, identical deposition conditions were used for the two cathodes, one deposited directly on the metal substrate, and the other deposited on top of the electrolyte. The APS parameter values used for the cathode deposition were based on conditions previously identified as giving a desirable electrode microstructure [7]. All of the deposited cathodes had an average thickness of approximately 50 μm and contained approximately 35 vol.% YSZ and 65 vol.% LSM as determined from EDX measurements. In order to achieve the high density required in the electrolyte layer, its deposition was carried out in a high energy plasma (87 kW) using 100% N_2 with 250A/cathode torch current at a standoff distance of 120 mm. The electrolytes were produced with an average thickness of approximately 60 μm. The conditions used for the deposition of the cathodes and the electrolyte in the symmetric cells can be seen in Table 1.

2.2. Characterization and testing

The substrate surface and cross-sections of the deposited cells were examined by scanning electron microscopy (SEM) to eval-

Table 1
Plasma spray parameters used for deposition of cathode layers in four symmetric cells prepared for electrochemical testing

	Cathode	Electrolyte
Standoff distance (mm)	100	120
Plasma gas flow rate (slpm)	250	150
Plasma composition	23% Ar, 77% N_2	0% Ar, 100% N_2
Carrier gas flow rate (slpm)	11.7	20
Arc current (A/cathode)	183	250
Powder size (LSM/YSZ) and (YSZ)	−45 + 32 μm/−45 + 32 μm	−25 μm
Feed rate (g min^{-1})	40	20
Nozzle diameter (mm)	12.7	9.52

uate and compare the coating microstructures. Energy dispersive X-ray spectroscopy (EDX) was used to identify the elements present in the coatings and substrate.

Electrochemical characterization of the symmetric cells was carried out using EIS measurements (SI 1260 frequency response analyzer, Solartron Analytical, Farnborough, UK) at temperatures between 500 °C and 900 °C to measure the series (R_s) and polarization resistance (R_p) of the cells. Tests were performed in an air atmosphere with a total flow rate to both cathodes of 0.1 slpm. Impedance measurements were carried out at OCV with an ac voltage amplitude of 20 mV over a range of frequencies between 1 MHz and 0.1 Hz. Electronic dc short circuit resistance across the cell between room temperature and 900 °C was measured by means of a digital multi-meter across the test stand leads. Circuit modeling and simulation was performed using ZView software (Scribner Associates, Southern Pines, NC, USA).

3. Results and discussion

3.1. Microstructural properties

SEM microscopy of the 430SS substrates reveals the presence of many surface pores of irregular shapes and sizes, as seen in Fig. 1. Some of these pores have individual dimensions approaching 100 μm, larger than the average diameter of powder particles being deposited. As a consequence, the molten particles are unable to span some of these gaps and instead fill up these pores, leaving large gaps in the surface of the cathode layer, as seen in Fig. 2. As is the case in the cell shown in Fig. 2, often the subsequently deposited electrolyte layer is able to be deposited in a continuous layer over the depression created by the substrate pore. However, in some cases the geometry of the substrate pore is such that sharp discontinuities in the cathode and electrolyte layers result, as shown in Fig. 3. Flaws such as these in the electrolyte expose the underlying cathode, allowing it to come into direct contact with a subsequently deposited electrode layer. This electrode can be either another cathode, in the case of symmetric cells produced for cathode research

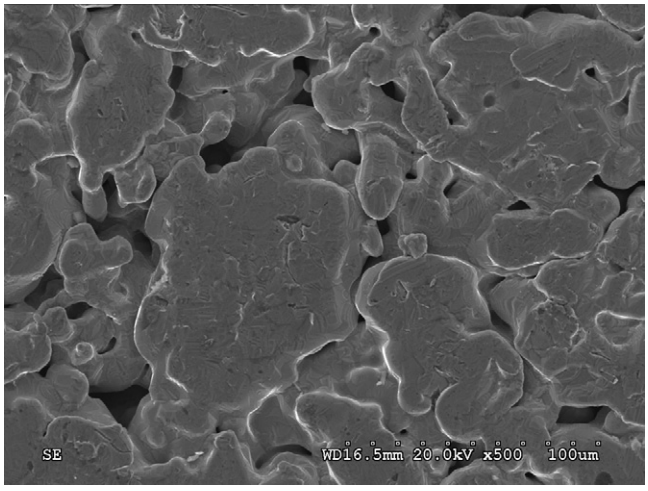

Fig. 1. SEM micrograph showing top surface of 430SS substrate.

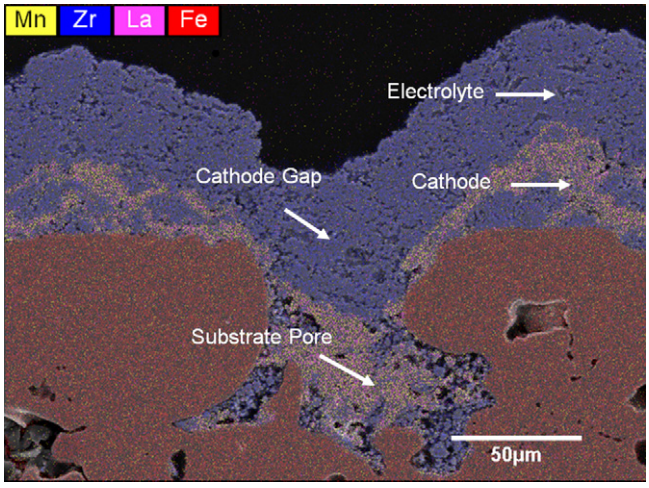

Fig. 2. EDX map of a polished cross-section of an air plasma sprayed cathode and electrolyte on a 430SS substrate showing a gap in the cathode layer resulting from a large substrate pore, underneath a continuous electrolyte layer.

and development, or an anode, in the case of full cells. This contact creates an electronic pathway between the electrodes, effectively short circuiting the electrolyte. The conductance of this short circuit path depends on the intrinsic conductivity of the electronically conducting cathode material, LSM in this case, at the temperature being examined, on the thickness of the SOFC, and on the area of contact between the electrodes.

3.2. Electrochemical evaluation

The short circuit resistance was found to vary significantly amongst cells produced using nominally identical conditions, due to the stochastic nature of the occurrence of substrate pores sufficiently large to cause a break in the electrolyte layer. Measured short circuit resistance was found to range from several kilo-ohms up to several mega-ohms. The short circuit resistance in one of the cathode symmetric cells produced, as measured over two thermal cycles, can be seen in the Arrhenius plot

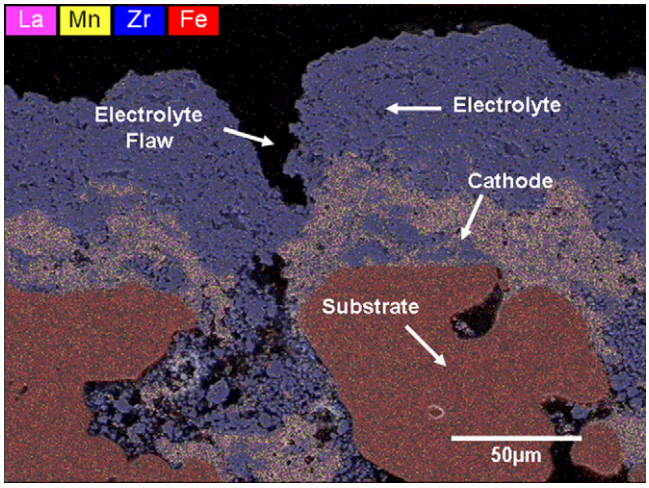

Fig. 3. EDX map of a polished cross-section of an air plasma sprayed cathode and electrolyte on a 430SS substrate showing an electrolyte flaw resulting from a discontinuity caused by the presence of a deep substrate pore.

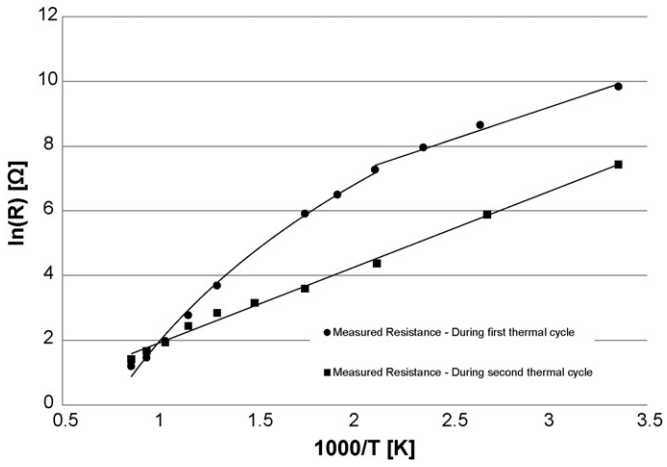

Fig. 4. Arrhenius plot showing measured electronic short circuit resistance across a cathode symmetric cell over two cycles between 25 °C and 900 °C.

in Fig. 4. At room temperature, the short circuit resistance of this as sprayed cell prior to being thermally cycled was found to be 18 kΩ. The decrease in ln(resistance) with temperature appears to be nearly logarithmic ($R^2 = 0.996$), with the resistance decreasing more quickly with increasing temperature than expected based solely on the increase in LSM conductivity with temperature, particularly at temperatures above 300 °C. The measured electronic dc resistance across the cell at 900 °C was 3.3 Ω.

This unexpectedly rapid decrease in resistance was found to be non-reversible as, upon cooling back to room temperature, the measured resistance was found to be just 1.7 kΩ, more than an order of magnitude lower than in the as sprayed cell. Upon reheating the cell back up to 900 °C, the decrease in short circuit resistance was found to be much closer to the expected Arrhenius behaviour, with an activation energy of 0.2 eV, which is within the range of the literature values reported for the activation energy associated with electronic conductivity in LSM [8]. A resistance of 4.1 Ω was measured at 900 °C during the second cycle. Upon cooling back to room temperature, the measured short circuit resistance was found to be unchanged from its value after the first cycle. This same pattern was observed in all of the cells tested, albeit with different values for the short circuit resistance.

The most likely explanation for the observed rapid decrease in short circuit resistance during initial thermal cycling of the cell followed by stabilization on subsequent cycles is as the consequence of an increase in the area of contact between the two electrodes due to sintering. This sintering takes place between the particles from the two electrodes in contact through gaps in the electrolyte. As some sintering begins to take place at the elevated temperatures, the contact between these particles becomes more intimate, increasing the area short-circuited as a result. This effect is illustrated in Fig. 5. The magnitude of area increase was estimated by comparing the expected short circuit resistance behaviour of the sprayed cell (i.e. the extrapolation of the low-temperature Arrhenius behaviour of the cell using the measured room-temperature short circuit resistance value) and the actual measured short circuit resistance of the cell after thermal cycling. The chart in Fig. 6 shows the approximate increase in electrode contact area as a function of temperature during the first thermal cycle. There is some decrease in apparent contact area when the cell is cooled back down to room temperature, down from 16.4 times the initial area at 900 °C to 11.1. This could possibly be the result of a decrease in conductivity due to substrate oxidation or as the result of an actual decrease in contact area due to thermal shrinkage upon cooling down. On the second thermal cycle the area of contact remains relatively stable, with only small variations.

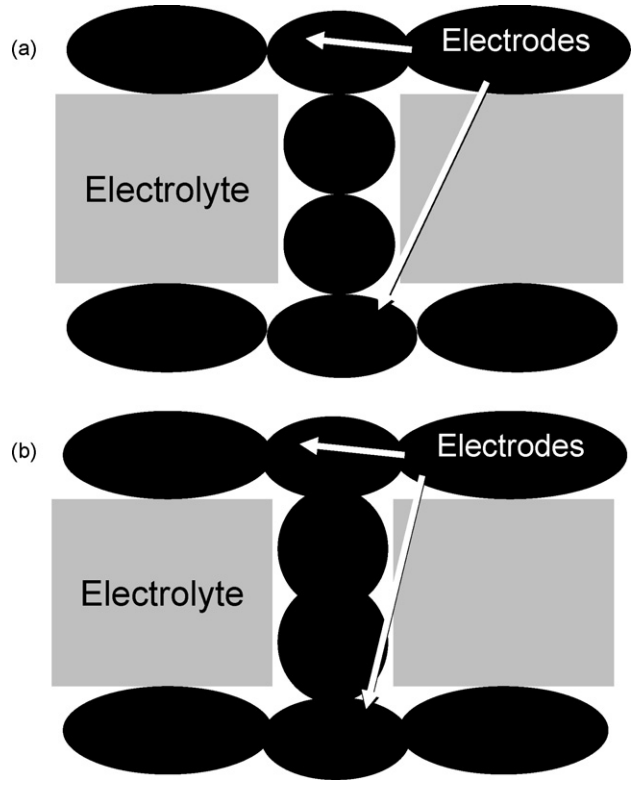

Fig. 5. Schematic showing the expected change in contact of plasma sprayed cathode particles through an electrolyte gap before (a) and after (b) thermal cycling.

Electrode R_p measurements performed by EIS during the first two thermal cycles on cells with short circuits also show

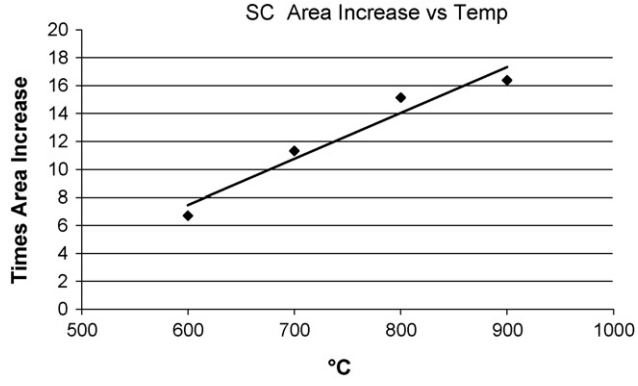

Fig. 6. Times increase in contact area between cathodes contributing to short circuiting over the first thermal cycle between 600 °C and 900 °C, assuming an activation energy for LSM conductivity of 0.2 eV.

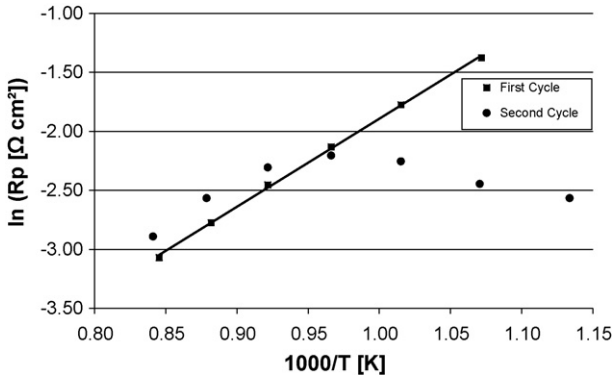

Fig. 7. Arrhenius plot showing the measured electrode R_p behaviour in a cell with a low short circuit resistance over two thermal cycles.

some significant differences. The observed R_p behaviour in cells with relatively low short circuit resistance, <50 Ω at temperatures above 300 °C especially, can exhibit ordinarily unexpected behaviour. An example of this behaviour can be seen in Figs. 7 and 8. The Arrhenius plot for the first thermal cycle of this cell appears normal, though with an activation energy of 0.64 eV, which is at the low end of values typically reported for LSM-based cathodes [9–11]. However, on the second thermal cycle, the trend in R_p appears quite different, particularly at temperatures below 750 °C. At lower temperatures, the R_p actually appears to decrease, which normally suggests an improved electrode performance, as temperature goes down. However, this change in behaviour is actually the result of the large decrease in short circuit resistance that occurs between the first and second thermal cycle. In cells with a short circuit with relatively low electronic resistance compared to the ionic resistance of the electrolyte, determination of the diameter of the Nyquist impedance arc derived from EIS testing is no longer a reliable method for determining the electrodes' R_p.

An SOFC possessing an electronic short circuit between electrodes can be described by the equivalent circuit shown in Fig. 9. The high-frequency intercept (HFI) and low-frequency intercept (LFI) on the Nyquist plot of such a cell measured by EIS can be described by the following expressions:

$$\mathrm{HFI} = R_{\mathrm{contact}} + R_{\mathrm{ic}} + \frac{R_e R_{sc}}{R_e + R_{sc}} \tag{1}$$

$$\mathrm{LFI} = R_{\mathrm{contact}} + R_{\mathrm{ic}} + \frac{R_{sc}(R_{p,c} + R_e + R_{p,a})}{R_{p,c} + R_e + R_{p,a} + R_{sc}} \tag{2}$$

The "apparent" polarization resistance for the cell electrodes, as determined from the Nyquist plot, would therefore be

$$\mathrm{LFI} - \mathrm{HFI} = R_{p,c}^{\mathrm{app}} + R_{p,a}^{\mathrm{app}} = \frac{R_{sc}(R_{p,c} + R_e + R_{p,a})}{R_{p,c} + R_e + R_{p,a} + R_{sc}} - \frac{R_e R_{sc}}{R_e + R_{sc}} \tag{3}$$

or

$$R_{p,T}^{\mathrm{app}} = R_{p,c}^{\mathrm{app}} + R_{p,a}^{\mathrm{app}} = \frac{R_{sc}^2(R_{p,c} + R_{p,a})}{(R_e + R_{sc})(R_{p,c} + R_e + R_{p,a} + R_{sc})} \tag{4}$$

From this expression, it can be seen that depending on the values of R_{sc} and R_e, apparent R_p and actual electrode R_p can have radically different values. In the simplest example, with real $R_{p,T}$ and R_e fixed at 1 Ω, Fig. 10 shows how the ratio of apparent $R_{p,T}^{\mathrm{app}}$ to real $R_{p,T}(=R_{p,c}+R_{p,a})$ changes with R_{sc}. It can be seen by this example that low values of R_{sc} can cause very large differences between apparent and real R_p. As R_{sc} increases towards infinity, corresponding to a cell with no short circuit, the apparent R_p converges to the real value, as expected.

These expressions can be rearranged to allow the real cell parameters R_e, $R_{p,c}$, and $R_{p,a}$ to be determined from their apparent values and R_{sc} as follows:

$$R_e = \frac{-R_{sc} R_e^{\mathrm{app}}}{R_e^{\mathrm{app}} - R_{sc}} \tag{5}$$

and

$$R_{p,c} + R_{p,a} = \frac{-(R_e + R_{sc})^2 (R_{p,c}^{\mathrm{app}} + R_{p,a}^{\mathrm{app}})}{(R_{p,c}^{\mathrm{app}} + R_{p,a}^{\mathrm{app}})(R_e + R_{sc}) - R_{sc}^2} \tag{6}$$

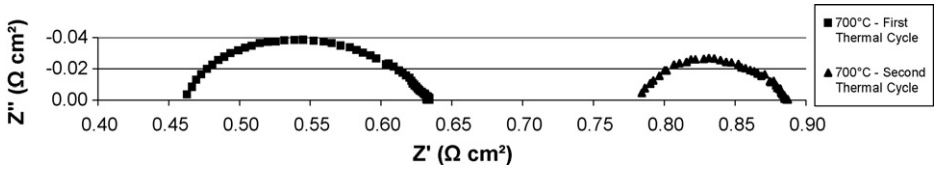

Fig. 8. Nyquist plots showing the measured electrode impedance of a cell with a low short circuit resistance over two thermal cycles at 700 °C.

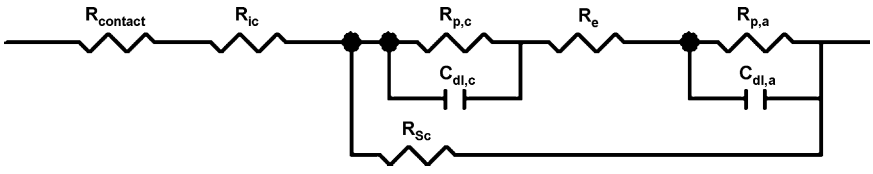

Fig. 9. Equivalent circuit model for a full cell possessing an electronic short circuit between electrodes. The circuit has the following components—R_{ic}: interconnect resistance; $R_{contact}$: contact resistance between cell and test stand; $R_{p,c}$: cathode polarization resistance; $R_{p,a}$: anode polarization resistance; $C_{dl,c}$: cathode double layer capacitance; $C_{dl,a}$: anode double layer capacitance; R_e: electrolyte ionic resistance; R_{sc}: electronic short circuit resistance.

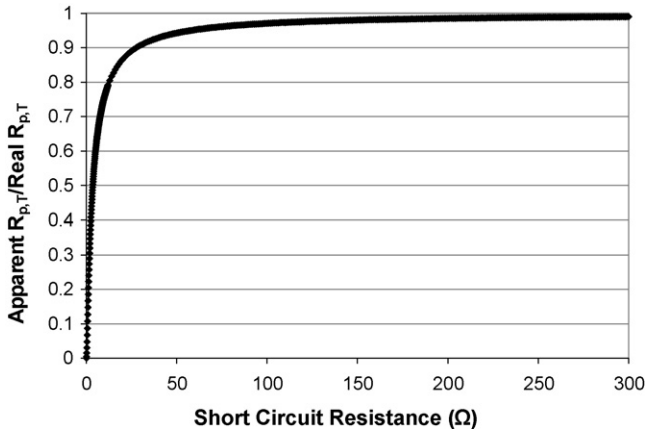

Fig. 10. Plot showing ratio of apparent to real $R_{p,T}$ as a function of R_{sc} when real $R_{p,T}$ and R_e are fixed at 1 Ω.

In Eq. (5), R_e^{app} would normally be taken as the value of the HFI minus any known contact resistance and interconnect resistance. However, it can be very difficult to determine a value for R_e^{app} unless accurate values for $R_{contact}$ and R_{ic} are known, which in practice is often not possible. This can make determining real R_p values problematic in actual experimental setups. On the other hand, if all of these parameters are known, then it is possible to accurately determine the electrodes' performance from the EIS data.

In a typical cell, the difference between R_p and R_p^{app} will be much larger at lower temperatures, leading to the abnormal behaviour observed in Fig. 7. Table 2 shows these values calculated at 500 °C and 900 °C for one of the cathode symmetric cells prepared by APS, using measured values for R_{sc} and reasonable estimates for R_e, R_{ic}, and $R_{contact}$. In this case R_p is almost six times larger than R_p^{app} at 500 °C, while R_p is only approximately 10% larger than the apparent value at 900 °C. The difference in this effect at high and intermediate temperatures is related to the large differences in activation energy between the electronic conductivity in the electrodes, upon which the short circuit resistance is dependent, and the ionic conductivity of the electrolyte. The difference between R_p and R_p^{app} is much greater when R_{sc} is small compared to R_e. As temperature increases, R_e declines much faster than R_{sc} due to the much higher activation energy for conductivity of YSZ compared to that of LSM (~0.9 eV vs. ~0.2 eV), leading to relatively much smaller values for R_e compared to R_{sc}. Conversely, as temperature decreases, R_e increases much more quickly than R_{sc}, causing R_p^{app} to appear much smaller than R_p.

Table 2
Results of calculations to determine $R_{p,c}$ in a cathode symmetric cell prepared by APS. Values calculated at 500 °C and 900 °C based on measured values for R_{sc} and $R_{p,c}^{app}$ and estimated values of R_e based on YSZ conductivity and thickness estimated from scanning electron micrographs

	500 °C	900 °C
R_{sc} (Ω cm^2)	15.5	2.4
R_e (Ω cm^2)	5.3	0.06
$R_{p,c}^{app}$ (Ω cm^2)	4.0	0.09
$R_{p,c}$ (Ω cm^2)	23.4	0.102

3.3. Manufacturing process solutions

Of course ultimately, it is important to fabricate cells without a short circuit. Diagnosis of a short circuiting problem by observation of the electrochemical behaviour demonstrated here can be utilized in order to identify the cause for a lower than expected cell performance, which in turn can be used to improve the cell structure and performance. To this end the manufacturing processes utilized in this study have been improved by making use of the diagnostic information determined from the short-circuited cells to greatly reduce the chance of a fabricated cell having a significant short circuit. This has been achieved primarily by the use of a combination of more energetic plasma conditions and finer YSZ powder in both the electrolyte and cathode layer. These changes have increased the ability of the electrolyte layer to more reliably fill any depressions caused by the filling of the metallic substrate surface pores with a portion of the cathode layer, and they have also resulted in smaller partially melted YSZ particles in the composite LSM–YSZ cathode layers, which in turn facilitates more uniform coverage of the cathode by the electrolyte layer. Furthermore, as the root of the problem relates to the large, irregularly shaped pores present in the steel substrate, finding an improved substrate having a finer, more uniform surface pore structure is highly desirable. Work is underway to develop APS cells using such improved substrates.

4. Conclusions

The presence of a short circuit between electrodes in an air plasma sprayed SOFC can dramatically affect the results of EIS testing, leading to a significant underestimation of R_p and hence an overestimation of electrode performance. This effect is particularly noticeable when testing at low temperatures, at which the ionic resistance of the electrolyte tends to be a larger fraction of the short circuit resistance than at higher testing temperatures. The short circuit in cells prepared using this fabrication method appears to arise from the presence of large, irregular pores in the surface of the porous stainless steel supports used as substrates for deposition. These large pores can cause discontinuities in the subsequently deposited cathode and electrolyte, allowing some of the top electrode to come into direct contact with the bottom cathode, creating an electronic pathway bypassing the electrolyte. Sintering, which takes place during the initial thermal cycling of the cell, appears to increase this contact area and to decrease the short circuit resistance significantly. Data from the EIS measurements of these cells, along with knowledge of the electrolyte and short circuit resistance, allow one to determine the real R_p values of the electrodes. Diagnostic information presented here regarding the source of the observed differences from expected electrochemical performance have allowed the modification of the plasma spray processing method being used to produce the SOFC layers that has led to the elimination of the short circuiting phenomenon through improvements to the electrolyte and cathode layers and to the substrates.

Acknowledgements

The authors gratefully acknowledge the generous financial support of Northwest Mettech Corp. and the Natural Sciences and Engineering Research Council of Canada and the assistance of Mr. David Waldbillig with scanning electron microscopy.

References

[1] G. Schiller, R. Henne, M. Lang, M. Muller, in: T. Candra, J.M. Torralba, T. Sakai (Eds.), Thermec' 2003: International Conference on Processing & Manufacturing of Advanced Materials, July 7–11, 2003, Leganes, Madrid, Spain, Trans Tech Publications Ltd., 2004, pp. 2539–2544.
[2] M. Lang, T. Franco, G. Schiller, N. Wagner, J. Appl. Electrochem. 32 (2002) 871–874.
[3] K. Barthel, S. Rambert, in: W.A. Kaysser (Ed.), Proceedings of the Fifth International Symposium on Functionally Graded Materials, October 26–29, 1998 (Dresden, Germany), Trans Tech Publications Ltd., 1998, pp. 800–805.
[4] B.D. White, O. Kesler, Adv. Mater. Res. 15–17 (2007) 299–305.
[5] M.L. Liu, H.X. Hu, J. Electrochem. Soc. 143 (1996) L109–L112.
[6] H.X. Hu, M.L. Liu, Solid State Ionics 109 (1998) 259–272.
[7] B.D. White, O. Kesler, L. Rose, Proceedings of the 10th International Symposium on Solid Oxide Fuel Cells (SOFC-X), June 3–8, 2007, Nara, Japan, ECS Transactions, vol. 7, 2007, pp. 1107–1114.
[8] N.Q. Minh, T. Takahashi, Science and Technology of Ceramic Fuel Cells, Elsevier, Amsterdam, 1995, pp. 1–14.
[9] K. Barthel, S. Rambert, Proceedings of the Third European Solid Oxide Fuel Cell Forum, 1998, Nantes, France, 1998, pp. 11–18.
[10] A. Barbucci, R. Bozzo, G. Cerisola, P. Costa magna, Electrochim. Acta 47 (2002) 2183–2188.
[11] S.P. Jiang, Solid State Ionics 146 (2002) 1–22.